Efficient Low-Lift Cooling with Radiant Distribution, Thermal Storage, and Variable-Speed Chiller Controls— Part I: Component and Subsystem Models

P.R. Armstrong, PhD
Member ASHRAE

W. Jiang, PhD

D. Winiarski
Associate Member ASHRAE

S. Katipamula, PhD
Member ASHRAE

L.K. Norford, PhD
Member ASHRAE

R.A.Willingham
Student Member ASHRAE

Component and subsystem models used to evaluate the performance of a low-lift cooling system are described. An air-cooled chiller, a hydronic radiant distribution system, variable-speed control, and peak-shifting controls are modeled. A variable-speed compressor that operates over 20:1 speed range and pressure ratios ranging from one to six is at the heart of the chiller. Condenser fan and chilled-water pump motors have independent speed controls. The load-side distribution is modeled from the refrigerant side of the evaporator to the conditioned zone as a single subsystem controlled by chilled-water flow rate for a specified instantaneous cooling load. Performance of the same chiller when operating with an all-air distribution system is also modeled. The compressor, condenser fan, and chilled-water pump motor speeds that achieve maximum coefficient of performance (COP) at a given condition are solved at each point on a grid of load and outdoor temperature. A variable-speed dehumidification subsystem is modeled and simulated as part of a dedicated outdoor air system to condition the ventilation air. A companion paper evaluates the annual cooling system energy use and potential energy savings to be gained by integrating radiant cooling, cool storage, and variable-speed compressor and transport motor controls.

INTRODUCTION

Significant improvements to cooling system efficiency can be achieved by integrating what we will refer to as the *low-lift cooling technologies*: 1) variable-speed compressor and transport motor controls, 2) radiant cooling with dedicated ventilation air dehumidification and distribution, and 3) cool storage. The energy requirements of all combinations of presence or absence of the foregoing three low-lift elements (Cases 1–8) are presented in a companion paper (Armstrong et al. 2009). This paper describes the component and subsystem models needed to estimate cooling system performance of the eight cooling system configurations over a wide range

P.R. Armstrong is an associate professor of mechanical engineering at Masdar Institute of Science and Technology, Abu Dhabi, United Arab Emirates. **W. Jiang** and **D. Winiarski** are senior research scientists and **S. Katipamula** is a staff scientist at Pacific Northwest National Laboratory, Richland, WA. **L.K. Norford** is a professor of building technology and **R.A. Willingham** is a graduate student in mechanical engineering at Massachusetts Institute of Technology, Cambridge, MA.

of balance-of-plant performance (standard-[1], mid-, and high-performance buildings) and a wide range of climate conditions.

The paper begins with an assessment of simulation requirements. Compressor, condenser, and evaporator component models are developed. Transport energy models are also developed for the condenser air side and the chilled-water loop. A special model is developed to represent a radiant ceiling panel array, the evaporator, and the chilled-water loop as a single subsystem. An idealized storage model that reduces computational effort and broadly addresses the potential energy saving role of thermal energy storage (TES) is described. Chiller and dedicated outdoor air system (DOAS) subsystem models and methods of simultaneously solving the component states and control actions needed to satisfy loads under any given condition with minimal input energy are presented. The method of representing a subsystem's performance map by one or more biquadratic or bicubic functions is described, and the role of the performance map within the peak-shifting optimal control algorithm is documented. Two-speed chiller performance is estimated by computing duty fraction after evaluating the bicubic at half- and full-capacity operating points. The paper concludes with a summary of the modeling process and some remarks about variable-speed chiller system performance. The main contribution of this work is the simultaneous optimization of chiller and distribution system operation over a wide range of lift and capacity fraction using a new semi-empirical positive-displacement compressor model and first-principles models of most of the other components.

SIMULATION REQUIREMENTS

To estimate annual energy consumption of a building that uses the baseline HVAC[1] configuration, the full low-lift system configuration, or some partial low-lift configuration, an appropriate simulation framework and accurate component or subsystem models are needed. Several issues must be addressed to obtain meaningful estimates of energy savings:

- supervisory control of chiller capacity and thermal energy storage must be near optimal
- compressor speed, distribution, and heat rejection flow rates must be controlled so as to maximize COP[2] over the entire domain of cooling load and outdoor condition
- HVAC configuration models (Cases 1–8) must provide for fair performance comparisons
- for each HVAC configuration, the corresponding chiller model must be consistent over wide ranges of capacity fraction and conditions

The computational burden of chiller dispatch with a 24-hour look-ahead controller is central to the formulation of subsystem and component models. Optimal control of thermal energy storage is a multidimensional, nonlinear search problem. It is solved by evaluating equipment performance and storage inventory many times in the search for a least-cost dispatch sequence over a specified control horizon. The choice of search technique may substantially affect computation time but even the best technique will suffer if the embedded performance models are not sufficiently accurate and efficient.

The control of variable-speed fans, pumps, and compressors presents another search problem. In contrast to the chiller-storage scheduling problem, an off-line optimization process may be used, and the resulting optimally controlled chiller or HVAC subsystem may be represented in the main simulation by a function that maps optimal performance over conditions and loads.

---

[1]*ANSI/ASHRAE/IESNA Standard 90.1-2004, Energy Standard for Buildings Except Low-Rise Residential Buildings.*
[2]That is, compressor, pump, and fan speeds, which are independently controlled, must produce maximum COP achievable for each distribution type (variable air volume [VAV] or radiant ceiling panel [RCP]) over entire capacity fraction and outdoor temperature domains.

The models used to simulate the components of the eight HVAC configurations (cooling and associated transport equipment) must be comparable in an engineering sense. To satisfy this requirement, identical component models are used for fans, pumps, compressors, condensers, and evaporators that are common to the eight HVAC configurations. Also, the same component models, with appropriate adjustment of parameters, are used for chiller, refrigerant-side econo- mizer, and dehumidification equipment.

The accuracy of component and subsystem models over all possible conditions and capacity fractions is another requirement. Many simulation programs treat solar radiation, envelope compo- nents and their integration, and schedules pertaining to occupancy, thermostat set points, internal gains and equipment operation in great detail while relying on manufacturer performance curves for HVAC equipment models. Performance data for chillers and compressors, fans, pumps, and heat exchangers are typically limited to the operating regions of most concern to designers: that is, the regions of moderate to heavy load and extreme conditions. For reliable performance assess- ment over a wide range of lift and capacity fraction, models based entirely on first principles, or models that reflect the basic physics with parameters inferred from credible published data, are developed. Refrigerant properties must also be accurately represented so that the comparison of two systems with distinctly different dominant regions of operation is not biased.

The chiller and dehumidifier components modeled in the analysis are vapor-compression machines for which refrigerant properties must be evaluated accurately over a wide range of conditions.

In summary, to satisfy the foregoing simulation requirements, performance map models or mathematical models of the key components—chiller, DOAS, and radiant panels—have been developed over the widest possible range of conditions and load using detailed models. The chiller and storage dispatch optimization has been programmed to use building load sequences generated by the DOE-2.2 (Jacobs 2002) simulation program as input. Details of the component models are presented in the next several sections, and model integration and application are summarized in the concluding section.

THERMAL ENERGY STORAGE AND PEAK SHIFTING

Low-lift cooling will be attractive primarily to designers of high-performance buildings in which cooling loads (except for the metabolic component) will be half or less of those experi- enced in buildings built to current standards (ASHRAE 2004). For the purpose of assessing low-lift energy savings, we assume that the existing building mass is capable of absorbing the design-day cooling load with small room temperature excursions. In cases where bal- ance-of-plant performance does not satisfy this assumption, a designer can compensate by installing phase-change material (PCM) or additional interior mass, or by further reducing the design-day heat gains. Having achieved the necessary intrinsic TES by one or a combination of these efforts, we postulate that the storage process can be modeled adequately for scoping pur- poses by a very simple algorithm with the following properties:

- thermal storage carryover is limited to one day
- effect on daily load of small changes in average room temperature is negligible
- effect on chiller performance of small changes in room temperature is negligible
- storage losses are negligible

The foregoing properties result in an idealized TES that is practical and realistic in size but opti- mistic in efficiency. Some implementations that approach the postulated ideal TES are 1) a TES that uses a substantial mass and surface area of distributed PCM, 2) a discrete PCM storage with very low thermal and transport losses, 3) a well-stratified water storage system with very low ther-

mal and transport losses, and 4) heavy constructions with decks exposed on both sides, double wallboard partitions, and high-performance envelope. Use of an idealized TES results in a simple statement of the optimal supervisory control problem as developed below.

The peak-shifting controller must find the time-shifted cooling load trajectory that minimizes input energy, given a building cooling load trajectory and the performance characteristics of a chiller and associated mechanical (transport) equipment. It is assumed that the 24-hour cooling load can be forecast with perfect accuracy (Henze and Krarti 1999). The situation is further simplified by using energy, not energy cost, as the objective function. This approach is generally most sensitive to equipment part-load performance. Given a reliable and complete chiller performance map, the sequence of 24 hourly chiller cooling rates $Q(t)$ is sought, which minimizes daily chiller input energy given by the following objective function:

$$\text{Minimize} \quad J = \sum_{t=1}^{24} \frac{Q(t)}{\text{COP}(t)} \tag{1}$$

subject to just satisfying the daily load requirement

$$\sum_{t=1}^{24} Q_{Load}(t) = \sum_{t=1}^{24} Q(t)$$

and to the capacity constraints

$$0 \leq Q(t) \leq Q_{Cap}(T_x(t), T_z(t)) \qquad t = 1{:}24$$

where
COP $= f(T_x, T_z, Q)$ = chiller coefficient of performance (kW$_{th}$/kW$_e$)
T_x $=$ outdoor dry- or wet-bulb temperature
T_z $=$ cooling load source temperature—e.g., zone temperature
Q $=$ evaporator heat rate—positive for cooling (Btu/h, ton, or kW$_{th}$)
Q_{Load} $=$ building cooling load with no peak-shifting
Q_{Cap} $= f(T_x, T_z)$ = chiller cooling capacity at full speed operation

The $Q(t)$ constraint describes dispatch vector upper and lower bounds in just the form needed to cast the problem as a bounded, but otherwise unconstrained, search—which is advantageous in terms of reliable convergence and computational efficiency. Note that the idealized TES model involves no interaction between hourly cooling rate and indoor temperature; the indoor temperature trajectory for the TES cases is assumed to be the same as that for the baseline (no TES) case.

The vector of uniform hourly average cooling rates based on the total daily load works well as an initial search point:

$$Q(t)_{Initial} = \frac{1}{24} \sum_{t=1}^{24} Q_{Load}(t) \tag{2}$$

Given a building's hour-by-hour cooling load trajectory, the outdoor dry-bulb[3] temperature trajectory and a room temperature setpoint schedule, the optimization can be run throughout the whole year in 365 one-day blocks to find the hourly chiller cooling rates (the so-called *peak-shifted load trajectory*), which minimizes HVAC input energy for the year.

---

[3]One would instead use wet-bulb temperature if water-cooled chillers were the chosen application of interest.

The large number of function calls during the search for a solution to each of the 365 24-hour control horizons makes the peak shifting control problem a computationally intensive one. It is critical that the chiller efficiency function evaluate in an accurate, yet computationally efficient manner. Performing a search for the optimum compressor, condenser fan, and chilled-water pump speeds at each chiller operating point in the 24-hour search process is out of the question.

Therefore, the chiller optimization is performed once at each point on a predefined grid of operating conditions, and a response surface is fitted, represented by a function that can be evaluated in just a few floating-point operations, to the resulting performance grid. The chiller component models are described next, followed by a description of the formulation for optimal chiller operation, and, finally, by a description of the performance functions fit to optimal solution points on a predefined chiller performance grid.

CHILLER COMPONENT MODELS

Each chiller component is represented by a model. The component models that are formulated in a manner familiar to most readers (i.e., condenser, simple evaporator, fan, and pump) are briefly documented. Component models that depart, such as the compressor (whose model must return mass flow and input power over a wide range of pressure ratio and shaft speed for the low-lift application) are presented in greater detail.

Subsystem models are then developed. The chiller and radiant cooling subsystem (RCS) are modeled together as a single system responding to indoor and outdoor conditions and imposed cooling load with input power being the response of interest. Solution methods that determine the minimum system power required to satisfy a given cooling load for any given indoor and outdoor temperature are documented for the main chiller in compressor mode and in free cooling mode. The chiller with all-air distribution[4] uses a similar model and identical components, except that distribution goes only as far as the chilled-water loop. The main internal variables for all three of these subsystems (chiller-variable air volume [VAV], chiller-RCS, and chiller-RCS in free-cooling mode) are pump, fan, and compressor motor speeds, condenser and evaporator refrigerant saturation temperatures, and the fraction of the condenser devoted to de-superheating. The coefficients and a goodness-of-fit metric of the bicubic performance map used to represent each chiller system (chiller-RCS, chiller-RCS in free-cooling mode, chiller-VAV) are presented.

For the DOAS dehumidifier, the evaporator saturation temperature is determined by a separate model. Given evaporating temperature and condenser air-side flow rates, the compressor input power is then determined by a subsystem model that solves for condenser saturation temperature and compressor speed. The DOAS dehumidifier model does not require a performance map.

Compressor

The compressor model returns refrigerant flow rate and input power given shaft speed, inlet temperature, and inlet and outlet pressures. For this project, a model was developed based on data generated by a publicly available[5] sizing tool, in which is embedded a proprietary compressor model. A dataset was generated by this tool for shaft speeds of 900, 1100, 1300, 1525, and 1750 rpm; condensing temperatures of 80°F, 90°F, 100°F, 110°F, and 130°F (26.67°C, 32.22°C, 37.78°C, 43.33°C, and 54.44°C); evaporating temperatures of 30°F, 35°F, 40°F, 45°F, and 50°F (–1.11°C, 1.67°C, 4.44°C, 7.22°C, and 10.0°C); and evaporator superheat temperature difference of 0°R, 5°R, 10°R, and 20°R (0 K, 2.78 K, 5.56 K, and 11.1 K). The resulting hypergrid involves $5 \times 5 \times 5 \times 4 = 500$ performance evaluations used to characterize the compressor. A subset of points returned by the sizing tool is presented in Table 1. The

---

[4]A variable-air-volume (VAV) system serves as the all-air baseline system.

[5]www.carlylecompressor.com/corp/details/0,2938,CLI1_DIV24_ETI1240,00.html

lowest speed accepted by the sizing tool is 900 rpm, the highest evaporating temperature is 50°F (10°C), and the lowest condensing temperature is 80°F (26.67°C).

The range of saturation temperature difference of interest for low-lift cooling is 0 R to 50 R (0 K to 28 K), while the published range of saturation temperature difference is typically 30 R to 90 R (17 K to 50 K). Published performance data for variable-speed compressors typically cover a range of 2:1 to 3:1, but for efficient cooling with peak shifting controls, a speed range of at least 5:1 is needed.[6] Simple approximate models involving, for example, a constant compression exponent model or a mass-flow and input-power-proportional-to-shaft-speed model do not fit the published data very well even over the limited range of pressure ratio and shaft speed presented in Table 1. Compressor flow rate and input power models designed to extrapolate reliably to lift conditions and compressor speeds well below the ranges covered by published data have therefore been developed.

Compression with simultaneous heat transfer is frequently modeled as a polytropic process, Pv^n = constant, in which the polytropic exponent, n, is a function of refrigerant properties, pressure ratio, (P_o/P_i), and compressor design (Gosling 1980; Moran and Shapiro 1995; Popovic and Shapiro 1995; Stoecker 1982; Threlkeld 1970). The fact that internal heat transfer per unit of regrigerant mass flow rate is roughly proportional to the duration of the suction-compression-discharge-re-expansion cycle (Boeswirth and Milovanova 1998) means that n will also be a function of shaft speed.

Work of Compression. The compressor sizing tool cited in Table 1 gives mass flow rate, ρV, to four digits and compressor input power W to five digits, for a specified inlet temperature and pressure, pressure ratio, and rpm. The compressor inlet state (P_i, T_i, v_i, h_i, and s_i) is therefore known to the precision of the state equations and the outlet-inlet enthalpy difference may be evaluated, to the accuracy of the sizing tool, by

$$h_o - h_i = \frac{W}{\rho V}. \tag{3}$$

With P_o and h_o in hand, the remaining outlet state variables (T_o, v_o, and s_o) can be evaluated to reasonable precision, and a polytropic model can be obtained by nonlinear least squares. The polytropic model, as mentioned above, is based on the idea that there is some n such that Pv^n = constant. This model can be applied even though the actual compression path is unknown.[7] Thus, for a given compressor, refrigerant, shaft speed, inlet condition, and pressure ratio (P_o/P_i), there is some n such that

$$P_o v_o^n = P_i v_i^n. \tag{4}$$

There are three special processes, deviations that provide a sense of how a real process might be represented by a polytropic model:

- $n_{IG} = c_p/c_v$ for an ideal gas[8] in isentropic (adiabatic, reversible) compression
- $n_T = 1$ for ideal gas in isothermal compression (heat removed during compression)
- n_s for real gas undergoing isentropic compression

---

[6]For scoping purposes, the variable-speed compressor is assumed to operate reliably over a wide speed range of 20:1. Commercially available reciprocating, scroll, and rolling piston compressors commonly operate over a 3:1 to 5:1 speed range. A few permanent-magnet motor-driven positive displacement compressors operate over 6:1, and at least one commercially available belt-driven reciprocating compressor operates over a 9:1 speed range. A wider 20:1 speed range can be achieved by restricting low speed operation to low pressure ratio conditions and/or by modification of oil pump and oil return mechanisms. Another possibility (not modeled) is to use two compressors sized for 0.2 and 0.8 of total capacity with each operating over a conservative 4:1 speed range.

[7]That is, the unknown distribution of irreversibilities and unknown variation of refrigerant state along the path.

[8]Also approximately true for real gas in a well-superheated state or for any dry low-pressure-ratio process.

Table 1. Subset of Sizing Tool Data Used to Estimate Compressor Model Parameters

Speed	SST	SDT	SSH	ρV	Q	W	T_o	ρV	Q	W	T_o	P_o/P_i	COP
rpm	°F	°F	°F	lb_m/h	Btu/h	Btu/h	°F	kg/h	W	W	°C	(–)	(–)
900	30	80	0	2114	156784	20360	110	961	45951	5967.2	43.3	2.27	7.70
900	30	100	0	2007	136484	25998	139	912	40001	7619.6	59.4	3.02	5.25
900	30	130	0	1774	103260	30328	179	806	30264	8888.6	81.7	4.47	3.40
900	40	80	0	2584	193857	19553	104	1175	56816	5730.7	40	1.90	9.91
900	40	100	0	2476	170478	26859	133	1125	49964	7871.9	56.1	2.53	6.35
900	40	130	0	2233	131861	32870	172	1015	38646	9633.6	77.8	3.74	4.01
900	50	80	0	3118	236399	17797	98	1417	69285	5216	36.7	1.60	13.28
900	50	100	0	3011	209755	26953	127	1369	61476	7899.5	52.8	2.13	7.78
900	50	130	0	2764	165451	34920	167	1256	48491	10234	75	3.15	4.74
1330	30	80	0	3061	227023	34204	118	1391	66537	10025	47.8	2.27	6.64
1330	30	100	0	2906	197629	43675	149	1321	57922	12800	65	3.02	4.52
1330	30	130	0	2569	149520	50950	191	1168	43822	14933	88.3	4.47	2.93
1330	40	80	0	3742	280705	32848	110	1701	82270	9627.2	43.3	1.90	8.55
1330	40	100	0	3585	246853	45121	141	1630	72348	13224	60.6	2.53	5.47
1330	40	130	0	3233	190935	55219	183	1470	55960	16184	83.9	3.74	3.46
1330	50	80	0	4515	342306	29898	103	2052	100324	8762.6	39.4	1.60	11.45
1330	50	100	0	4360	303726	45280	134	1982	89017	13271	56.7	2.13	6.71
1330	50	130	0	4003	239573	58664	176	1820	70215	17193	80	3.15	4.08
1750	30	80	0	3986	295629	47726	122	1812	86644	13988	50	2.27	6.19
1750	30	100	0	3784	257352	60941	154	1720	75426	17861	67.8	3.02	4.22
1750	30	130	0	3345	194705	71091	197	1520	57065	20836	91.7	4.47	2.74
1750	40	80	0	4873	365534	45834	113	2215	107132	13433	45	1.90	7.98
1750	40	100	0	4668	321452	62958	145	2122	94212	18452	62.8	2.53	5.11
1750	40	130	0	4210	248635	77049	188	1914	72871	22582	86.7	3.74	3.23
1750	50	80	0	5880	445751	41717	105	2673	130642	12227	40.6	1.60	10.69
1750	50	100	0	5678	395511	63181	138	2581	115918	18517	58.9	2.13	6.26
1750	50	130	0	5212	311972	81855	180	2369	91434	23990	82.2	3.15	3.81

The last process is of particular interest because it accounts for real gas properties as well as the pressure ratio of the process. It is also of interest because isentropic compression is a reversible and therefore efficient compression process. Note that the polytropic exponent of a real (irreversible) compression process can be higher (because of internal dissipation) or lower (because of heat transfer) than the isentropic exponent. In reality, both forms of entropy generation (flow loss and heat transfer) are at play, and one can determine n only by detailed modeling or careful experiment (Boeswirth and Milovanova 1998). When n is greater than n_s, outlet temperature, pressure, enthalpy, and compression work are also greater—and conversely when n is less than n_s.

The isentropic exponent for a real process with a dry,[9] pure, real gas is defined in terms of the compression process end states. A simplification commonly used in compressor models is to define the process in terms of compressor inlet and outlet states, thus

$$n_s = \frac{\ln(P_o/P_i)}{\ln(v_i/v(P_o, s_i))} .$$ (5)

A model in which the ratio of polytropic to isentropic exponent is a function of pressure ratio and shaft speed, f, in seconds per rotation, is postulated:

$$n \sim n_s(C_{00} + C_{01}f + (C_{10} + C_{11}f)(P_o/P_i)^x)$$ (6)

The model parameters C_{ij} and x are selected to minimize the coefficient of variation (COV) of the energy balance (assuming no net heat exchange with ambient air)[10] given by

$$W = \rho V(h_o - h_i) ,$$ (7)

where

W = shaft work rate (returned by compressor sizing tool),
ρV = refrigerant mass flow rate (returned by sizing tool), and
h_i = inlet enthalpy corresponding to inlet conditions.

The outlet enthalpy, $h_o = h(P_o, v_o)$, is evaluated by the refrigerant state equations (NIST 2007) using the polytropic model (Equatons 4 and 6) to estimate the compressed vapor's specific volume given by

$$h_o \sim h(P_o, v_i(P_o/P_i)^{-1/n}) .$$ (8)

The values of the Equation 6 model parameters that minimize the COV of Equation 8 are given below:

$$n \sim n_s\{0.9508 + 0.002311f + (0.03226 + 0.002391f)(P_o/P_i)^{-0.7217}\}$$ (9)

The resulting polytropic exponent is plotted against pressure ratio and shaft speed in Figure 1, and the isentropic compression efficiency is plotted against pressure ratio and shaft speed in Figure 2. The polytropic exponent curves are in good agreement with the semi-empirical results presented in Figures 9–11 of Popovic and Shapiro (1995), and the isentropic efficiency curves are in general agreement with the experimental results given in Figures 5 and 6 of Villadsen and Boldvig (1981). The model estimates of enthalpy rise, $h_o - h_i$, are plotted against the sizing tool's values of shaft input work per unit refrigerant mass in Figure 3. Based on the foregoing qualities, it seems that the sizing tool's underlying model is representing internal heat transfer and flow losses in a reasonable manner. Efforts are currently underway by the MIT-MIST authors to carefully measure and characterize the polytropic exponent of a machine in the 5F compressor family over a wide range of pressure ratios and shaft speeds.

Volumetric Efficiency. At a given internal pressure ratio, P_d/P_s, a reciprocating compressor develops a suction volume flow rate, V, that is approximately linear in displacement rate (i.e.,

---

[9] The polytropic model is commonly used for dry compression and expansion processes but has also been applied (Singh et al. 1986) to two-phase (wet) compression. Equations 4 through 6 are intended only for dry compression.

[10] More rigorous treatment of jacket loss is not possible because the sizing tool does not indicate ambient conditions.
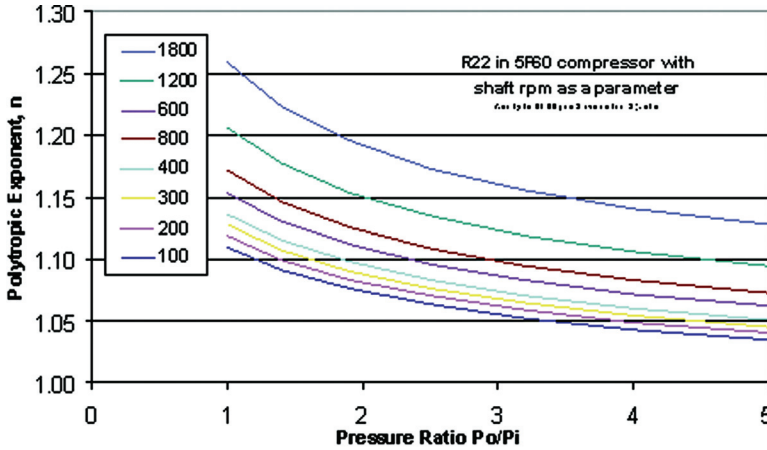
Figure 1. Polytropic exponent estimates, $n = n_s(C_{00} + C_{01}f + (C_{10} + C_{11}f)(P_o/P_i)^x)$, for compressor 5F60 with R-22, 50°F (10°C) saturated suction temperature and zero superheat.
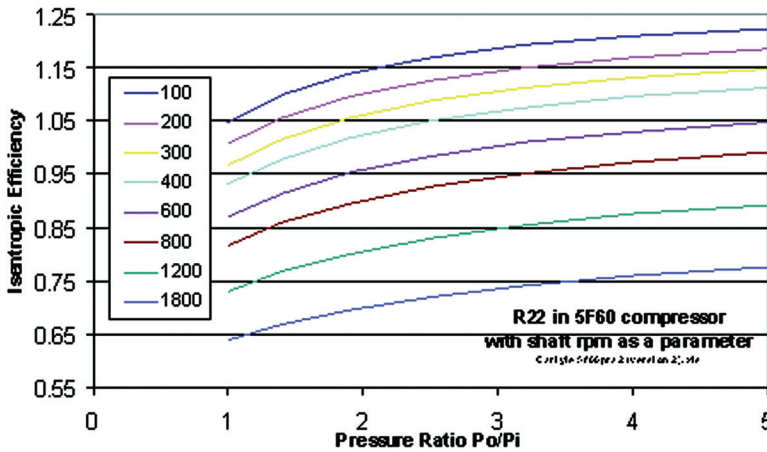

Figure 2. Compression efficiency for compressor 5F60 with refrigerant R-22 at 50°F (10°C) saturated suction temperature and zero superheat. The 800, 1200, and 1800 rpm curves correspond to sizing tool data; curves for lower shaft speed are based on the variable polytropic exponent model.

swept volume times shaft rotation frequency). However, the internal pressure ratio is greater than the external pressure ratio because of pressure drops across the suction and discharge valves, both of which are functions of flow rate. For purposes of estimating compressor performance for applications, an adjustment to the denominator of the pressure ratio has been found to adequately account for both suction and discharge flow loss (Gosling 1980; Jahnig et al. 2000; Popovic and Shapiro 1995; Stoecker 1982; Threlkeld 1970). Clearance volume reexpansion and pressure drop effects are thus reflected in a volumetric efficiency model of the following form:

$$\eta_{CV} = 1 + C - C\left(\frac{P_o}{P_s}\right)^{1/n}$$ (10)

where

$$P_s = P_i \exp\left(\frac{-C_{flow}\rho_i f^2}{P_i}\right)$$ (11)

and

C = ratio of effective clearance volume to displacement
P_s = discharge pressure assumed equal to outlet pressure
n = polytropic exponent given by Equation 9
C_{flow} = constant proportional to effective valve free area
ρ_i = inlet density
f = shaft speed in rotations per second

Other effects, such as leakage and heating, the latter of which reduces the suction gas density at the bottom of the suction stroke, have been treated empirically using a power law in shaft speed. The mass flow rate is thus modeled as

$$\rho V = f^x D \rho_i \eta_{CV} ,$$ (12)

where

x = empirical shaft speed exponent and
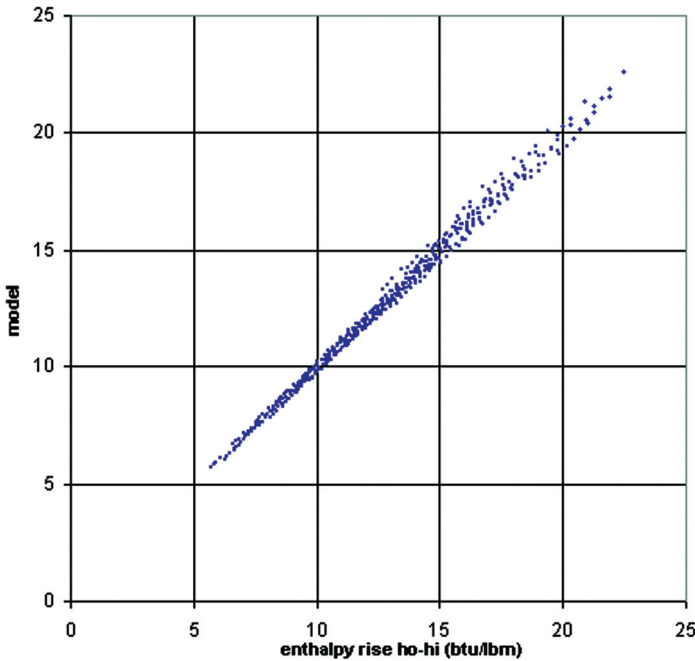D = effective or actual displacement.

Figure 3. Enthalpy rise, $h_o - h_i$, across the compressor: model versus sizing-tool data.

Because the sizing tool returns mass (not volumetric) flow rate, the parameters of Equations 10 and 12 must be solved together by substituting Equation 10 into Equation 12 and using the norm of Equation 12 residuals as the least-squares objective function. Table 2 shows the four model variants tested. The result with constraint $x = 1$ appears in Column A, and with constraint $C_{flow} = 0$, in Column B. The results with effective displacement constrained to actual displacement, $D_{actual} = 0.03409 \text{ ft}^3$, appear in Columns C and D with Column D again reflecting the $x = 1$ constraint. The model presented in Column C was used.

Condenser

Heat exchanger effectiveness models are used to describe evaporator and condenser performance. Single-phase and two-phase regions must be analyzed separately. The chiller system operates most efficiently with zero subcooling (i.e., liquid exiting the condenser in a saturated state because, for a given condenser UA and chiller load, zero subcooling results in the lowest condensing temperature and pressure).[11] In practice, some subcooling is unavoidable but by providing a liquid receiver tank at the condenser outlet, subcooling can be kept quite small if the condenser tube inside diameter is sufficient to maintain separate liquid and vapor phases (with vapor flow being essentially zero at the condenser outlet) under conditions in which the highest refrigerant flow rate is encountered. With zero subcooling assumed, the condenser model does not need to estimate what fraction of the condenser is in subcooling mode. The desuperheating section, however, comprises some initially unknown fraction, x, of the condenser's heat rejecting area.

To evaluate the fraction of the condenser needed for desuperheating, the enthalpy difference and temperature difference between the superheated discharge state and the saturated vapor at condensing pressure must be estimated. For this purpose, piping and condenser pressure drops are assumed to be negligible and the desuperheating load is thus given by

$$Q_{sh} = \rho V(h_o - h(T_c, P_o)) , \tag{13}$$

where $h(T_c, P_o)$ is the vapor enthalpy at the desuperheater exit, and T_c is the condensing temperature (temperature at the desuperheater exit).

The desuperheater section behaves as a cross-flow heat exchanger governed by the following:

$$Q_{sh} = \rho V(h_o - h_c) = \varepsilon C_{min}(T_{sh} - T_x) \tag{14}$$

Table 2. Parameters and COVs of Four Volumetric Efficiency Models

Parameter	Model			
	A	B	C	D
D	0.033335	0.039796	0.03409	0.03409
C	0.074928	0.086	0.075879	0.083298
C_{flow}	0.014189	0	0.012659	0.014911
f^x	1	0.93930	0.99221	1
COV	0.005147	0.002842	0.004512	0.010827

[11]Taking away part of the condenser for subcooling will raise pressure ratio, fan power, or both.

where

ε = cross-flow effectiveness, a function (Hiller 1976) of xUA_c and C_{min}
T_{sh} = compressor discharge temperature (superheated refrigerant vapor)
T_x = condenser air-side inlet (outdoor dry-bulb) temperature
C_{min} = the lesser of $\rho V(h_o - h_c)/(T_{sh} - T_c)$ and xC_c,
C_c = condenser air thermal capacitance rate mc_p
T_c = condensing temperature

In the condensing section, the heat balance is

$$Q_c = Q + W - Q_{sh} = \rho V(h_c - h_{liq}) = (1 - x)C_c\,(T_{LAT} - T_x)\,, \tag{15}$$

where

h_c = saturated refrigerant vapor enthalpy at P_o,
h_{liq} = saturated refrigerant liquid enthalpy at P_o,
C_c = condenser air thermal capacitance rate mc_p, (kW/K), and
T_{LAT} = condensing section leaving air temperature.

The leaving air temperature must also satisfy the heat exchanger equation,

$$\frac{T_{LAT} - T_c}{T_x - T_c} = \exp(-NTU_c)\,, \tag{16}$$

where

$NTU_c = UA_c/C_c$ = dimensionless condensing section capacity in number of transfer units and
UA_c = condenser conductance-area product based on average conductance (U is a function of airflow rate but has been taken as constant for scoping purposes).

Given entering refrigerant conditions and mass flow rate ρV, T_{sh}, and T_c and entering air temperature T_x, the unknown values of C_c and x are determined by successive approximation.

Evaporator Model for All-Air Distribution

When the chiller is used with an all-air distribution system, the chilled-water supply temperature must be low enough to control humidity. The supply temperature control schedule given in Appendix G of ASHRAE (2004) is typical of constant-volume (CV) as well as VAV all-air distribution systems. In application, the evaporator component model is given a cooling load and a trial value of the evaporating temperature. The model then determines the required chilled-water flow rate based on standard heat exchanger equations. The evaporator heat balance is

$$Q = \rho V(h_e - h_{liq}) = C_e(T_{cwr} - T_{cws})\,, \tag{17}$$

where

h_e = saturated refrigerant vapor enthalpy at evaporator pressure, P_i,
h_{liq} = saturated refrigerant liquid enthalpy at condenser pressure, P_o,
C_e = chilled-water thermal capacitance rate, mc_p,
T_{cwr} = chilled-water return temperature, and
T_{cws} = chilled-water supply temperature.

In flooded evaporator operation, there is zero superheat, and the chilled-water approach to evaporating temperature T_e is given by

$$\frac{T_{cws} - T_e}{T_{cwr} - T_e} = \exp(-NTU_e)\,, \tag{18}$$

where

$NTU_e = UA_e/C_e =$ dimensionless evaporator capacity and

UA_e = evaporator conductance-area product based on average conductance (kW/K) (U is a weak function of chilled-water flow rate, C_e), and from Equation 17, T_{cwr} is equal to $T_{cws} + Q/C_e$.

Negligible evaporator and suction line pressure drops are assumed so that the saturated suction temperature is equal to the evaporating temperature (i.e., the compressor inlet vapor is in a saturated condition). The evaporator model and chilled-water transport model (described later) allow the chiller solver to make the trade-off between evaporating temperature and chilled-water flow rate.

Radiant Cooling Subsystem (RCS)

An array of radiant cooling panels may be modeled by a heat exchanger effectiveness-NTU model with the zone-side condition modeled as a single temperature (Conroy and Mumma 2001). Because inlet temperature equal to outlet temperature implies, in effect, an infinite zone-side thermal capacitance rate, the heat exchanger's minimum thermal capacitance rate is always on the chilled-water side. The evaporator's minimum thermal capacitance rate is on the chilled-water side for the same reason.

The cooling panel array and evaporator are linked by chilled-water temperatures and flow rate. A combined evaporator-radiant panel model is derived below.

For zero superheat operation of the evaporator, the chilled-water supply temperature T_{cws} approach to evaporating temperature T_e is given by

$$\frac{T_{cws} - T_e}{T_{cwr} - T_e} = \exp\left(-\frac{UA_e}{C_e}\right) = e_e. \tag{19a}$$

The radiant ceiling panel array is a large heat exchanger with a hot-side temperature, T_z, roughly equal to zone operative temperature and roughly uniform over zone area. The chilled-water return temperature T_{cwr} approaches T_z as follows:

$$\frac{T_z - T_{cwr}}{T_z - T_{cws}} = \exp\left(-\frac{UA_z}{C_e}\right) = e_z \tag{20a}$$

where UA_z is the panel array conductance-area product (kW/K) based on average local conductance. (U, a function of chilled-water flow rate, has been taken as constant for scoping purposes.)

RCS Model. Equations 19 and 20 form a linear system in T_{cwr} and T_{cws}. The analytical expression for effective evaporator-to-zone conductance, $UA_{eff} = Q/(T_z - T_e)$, is derived in terms of its solution. First, multiply through by the denominators on the left to get

$$T_{cws} - T_e = e_e(T_{cwr} - T_e) \tag{19b}$$

$$\text{and} \quad T_z - T_{cwr} = e_z(T_z - T_{cws}) \tag{20b}$$

and move unknowns to the left to obtain the standard $Ax = b$ form:

$$T_{cws} - e_e T_{cwr} = (1 - e_e)T_e \tag{19c}$$

$$e_z T_{cws} - T_{cwr} = (1 - e_z)T_z \tag{20c}$$

Substituting Equation 19c into Equation 20c and vice versa yields the temperatures of interest

$$(1 - e_e e_z)T_{cws} = (1 - e_e)T_e + e_e(1 - e_z)T_z \tag{21}$$

$$\text{and} \quad (1 - e_e e_z)T_{cwr} = (1 - e_z)T_z + e_z(1 - e_e)T_e \tag{22}$$

and an expression for the chilled-water temperature difference:

$$T_{cwr} - T_{cws} = \frac{1 - e_e - e_z + e_e e_z}{1 - e_e e_z}(T_z - T_e) \tag{23}$$

The sensible cooling rate is given by

$$Q = C_e(T_{cwr} - T_{cws}) \, .$$

An effective conductance is defined for the evaporator-RCS assembly as

$$UA_{eff} = \frac{Q}{T_z - T_e} = C_e \frac{T_{cwr} - T_{cws}}{T_z - T_e} = C_e \frac{1 - e_e - e_z + e_e e_z}{1 - e_e e_z} \tag{24}$$

and is used to define the following useful dimensionless heat exchanger parameters:

$$u_e = UA_e/UA_{eff}$$

$$u_z = UA_z/UA_{eff}$$

$$c = C_e/UA_{eff}$$

The exponentials of Equations 19 and 20 may be evaluated using the foregoing dimensionless parameters:

$$e_e = \exp(-UA_e/C_e) = \exp(-u_e/c)$$

$$e_z = \exp(-UA_z/C_e) = \exp(-u_z/c)$$

The nondimensional chilled-water flow rate, c, is seen to satisfy

$$c = \frac{C_e}{UA_{eff}} = \frac{1 - e_e e_z}{1 - e_e - e_z + e_e e_z} \, . \tag{25}$$

Another useful relationship is the evaporator-to-zone infinite-flow thermal resistance:

$$\frac{T_z - T_e}{Q} = \frac{1}{UA_{eff}} + \frac{1}{UA_z} \tag{26}$$

Evaluation of C_e Given Cooling Load and Zone-Evaporator Temperature Difference.
The minimum chiller input power required to satisfy a given cooling load under given external conditions is determined iteratively with T_e and T_c as the primary unknowns. Cooling rate Q and T_e, T_c determine the mass flow rate of a given refrigerant that the compressor must deliver. Compressor speed and compressor input power are then evaluated via the compressor performance model. Chilled-water flow rate C_e is constrained by Equations 24 and 25, and thus (given cooling load, zone temperature, and T_e) is uniquely determined.

An upper bound on T_e is given by Equation 26, and a lower bound on T_c is given by a similar relation involving the condenser UA. Because these infinite-flow conditions, corresponding to infinite transport power, are clearly suboptimal, a small buffer (e.g., $0.001[T_{cLB} - T_{eUB}]$) may be added without fear of excluding an optimal solution from the search space.

Transport Flow and Input Power Models

The chiller system includes a variable-speed condenser fan and a variable-speed chilled-water pump. Transport power is determined by the chilled-water loop flow-pressure relation and the variable-speed chilled-water pump performance map. Condenser air-side flow rate and transport power are evaluated similarly. The transport models assume a load pressure drop that is approximately proportional to flow squared, a constant efficiency motor, a constant efficiency fan or pump, and flow rate that is approximately proportional to shaft speed (Granryd 1998). These assumptions lead to the following power-law models:

$$\text{Flow rate} = C_x = k_{FSx}(f_x/f_{xo}) \tag{27}$$

$$\text{Input power} = E_x = k_{PSx}(f_x/f_{xo})^3 \tag{28}$$

where f_x = shaft speed, $x = e$ signifies the chilled-water pump, and $x = c$ signifies the condenser fan.

The constants k_{FSx} and k_{PSx} may be evaluated at any operating point, typically at the pressure drop and flow rate developed when the motor is operated at rated speed f_{xo} and the corresponding pump or fan motor input power at this point. Power-law models based on actual fan and pump performance data and actual flow-pressure characteristics of the condenser air-side flow path and the chilled-water distribution network can be readily substituted.

OPTIMAL CHILLER OPERATION AND CHILLER PERFORMANCE MAPS

The chiller operating point is defined by cooling load Q and the boundary conditions, outdoor dry-bulb temperature T_x, and source temperature T_z for the chiller-RCS system or T_{cws} for the chiller-VAV system. The objective of static chiller control is to minimize chiller system power consumption at a given operating point. Although previous work has focused on centrifugal chillers or reciprocating chillers with cylinder unloaders (Braun et al. 1987a, 1987b, 1989a; Henze et al. 1997; King and Potter 1998), the same objective function applies to variable-speed chillers that use a positive-displacement compressor of the volume-index (scroll, screw) or free-discharge (reciprocating, rolling piston) types. Chiller system input power includes compressor, fan, and pump power, the sum of which is to be minimized at a given operating point as expressed by Equation 29:

$$\text{Minimize} \quad J = f(T_x, T_z, Q) = E_e + E_c + W/\eta_{motor} \tag{29}$$

where

$E_e \quad = \quad k_{PSe}(f_e/f_{eo})^3$ = chilled-water pump input power (kW) from Equation 28
$E_c \quad = \quad k_{PSc}(f_c/f_{co})^3$ = condenser fan input power (kW) from Equation 28
$W \quad = \quad$ compressor input power (kW) from Equation 7
$\eta_{motor} = \quad$ compressor motor and drive efficiency[12]

---

[12]A constant motor-drive efficiency of 0.94 was assumed. In practice, efficiency falls off moderately with load below about 35% to about 0.86 at 10% load (Baldwin 1988; Zhu 2006), but for scoping purposes, the constant $\eta_{motor} = 0.94$ assumption was applied to both variable and two-speed compressors.

Implicit[13] in the objective function are two unknowns—T_e and T_c, the evaporator and condenser saturation temperatures. The solution is constrained by $T_c > T_e$, and, for a given load, Q, is bounded by the evaporator saturation temperature at infinite chilled-water flow rate and the condenser saturation temperature at infinite condenser airflow rate. Evaporator transport fluid (chilled water) and condenser transport fluid (air) capacitance rates are approximately inversely proportional to the corresponding transport fluid temperature differences. The chilled-water thermal capacitance rate can be solved quickly and efficiently by successive approximation or by a bounded one-dimensional search. The condenser has an additional unknown: the fraction of area for desuperheating. Because 90% of the condenser is typically condensing, the air-side capacitance rate is mainly determined by condensing load, and both unknowns can be simultaneously solved in a single successive approximation loop. Thus, when feasible saturation temperatures T_e and T_c are specified, all other intermediate variables (the flow rates, shaft speeds, and electrical loads of fan, pump, and compressor) can be evaluated. The solver, given Q and feasible initial guesses of T_e and T_c, performs a search to find the values of T_e and T_c that minimize the total chiller system electrical load given by Equation 29.

Although the refrigerant and transport flow rates are solved internally, a map of chiller performance in the form of $1/COP = J/Q = f(T_x, T_z, Q)/Q$ is all that is needed to perform annual energy calculations. Hin (2002) reviewed a representative selection of first-principles, black-box, and hybrid chiller models used for system simulation. Neither hybrid nor black-box chiller models have been developed for the wide ranges of capacity modulation and pressure ratio needed by the low-lift application. To overcome this limitation, first principles models or semi-empirical models with speed (or associated flow rate) and pressure-ratio terms for all of the main components have been employed. The resulting system models produce sets of performance data valid over a wide range of capacity and lift. Black-box models based on these data sets then serve to represent chiller performance in the system simulation task.

Chiller RCS Performance Map

A map of chiller system input power was produced for an indoor temperature T_z of 72°F (22.22°C) on a grid of cooling load Q and outdoor temperature T_x. A set of input power versus cooling load curves was generated for each outdoor temperature. A bicubic (third-order bivariate polynomial) was fit to the surface. The bicubic accurately represents the chiller performance surface over a wide range of lift and capacity and is compatible with most simulation programs. The bicubic also satisfies the need of the 24-hour look-ahead controller for computational efficiency and for a power versus load function that is smooth (continuous first derivative).

Figure 4 shows the optimal chiller system performance map for $T_z = 72°F$ (22.2°C) with T_x ranging from 110°F to 50°F in 10°F increments (43.33°C to 10°C in 5.56 K increments). Note the inflections at low capacity fraction on the 50°F and 60°F (10.0°C and 15.56°C) outdoor temperature lines; the compressor is bypassed below these inflection points (see refrigerant-side economizer model). Table 3 documents the bicubic coefficients, and Figure 5 shows the model regression error for the seven curves covering the region of compressor operation. The economizer region performance map is addressed later.

Chiller VAV Performance Map

The chiller performance model for all-air (CV and VAV) applications differs from an RCS-plus-DOAS application with respect to chilled-water supply temperature. The chilled-water supply temperature reset schedule for all-air systems provided in Appendix G of *ANSI/ASHRAE/IESNA Standard 90.1-1999, Energy Standard for Buildings Except Low-Rise*

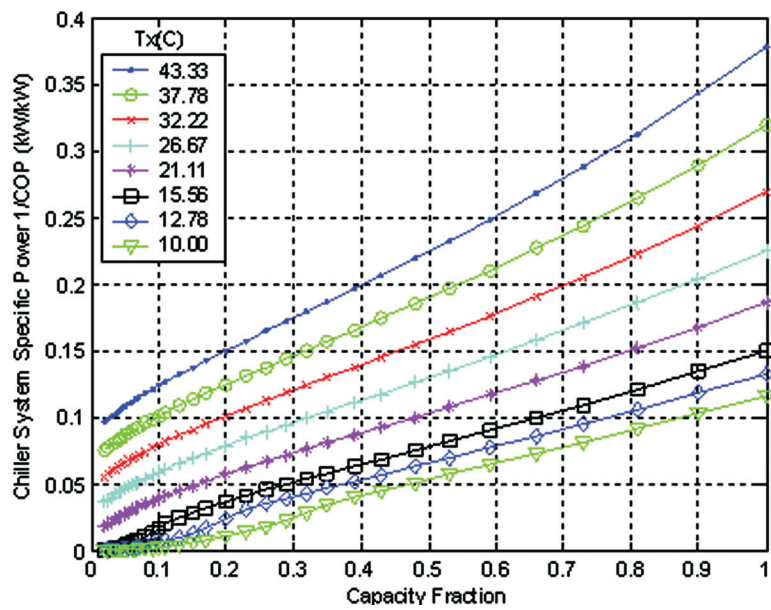[13]Via Equations 7–12 and the saturation pressure-temperature curve.

Figure 4. Chiller-RCS performance map at T_z =22.2°C (72°F) with T_x ranging from 43.33°C (110°F; topmost curve) to 10°C (50°F) in 5.56 K (10 R) increments.

Table 3. Bicubic Chiller Performance Map, $x = T_x$, y = Capacity Fraction; $r^2 = 0.9998$

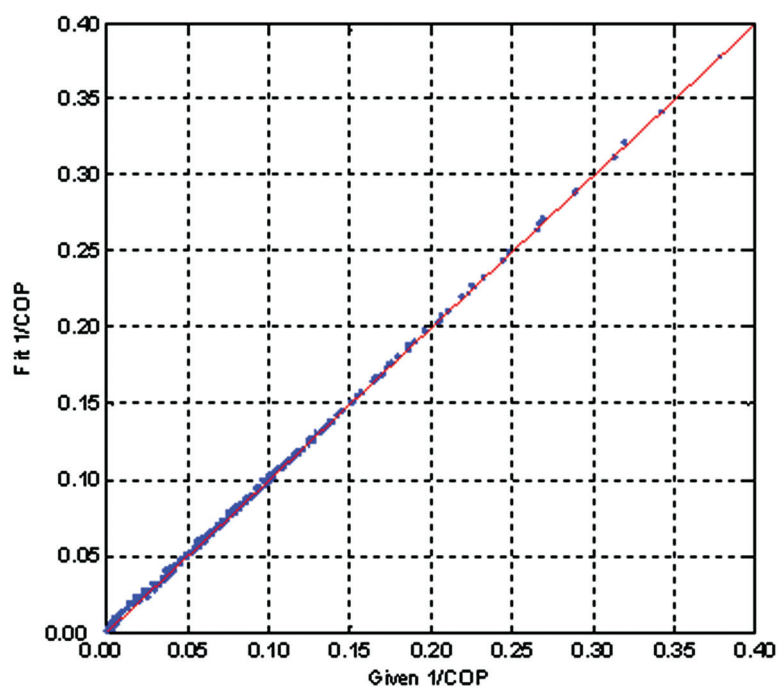|	Bicubic Coefficients	
Term	**(x in °F)**	**(x in °C)**
Constant	7.46E-02	−1.99E-01
x	5.44E-03	4.91E-03
y	2.53E-01	3.19E-01
x^2	7.27E-05	−3.64E-05
xy	2.29E-03	−2.85E-03
y^2	2.34E-01	−2.73E-01
x^3	8.47E-07	1.45E-07
x^2y	7.97E-05	2.46E-05
xy^2	2.21E-03	1.23E-03
y^3	1.18E-01	1.18E-01

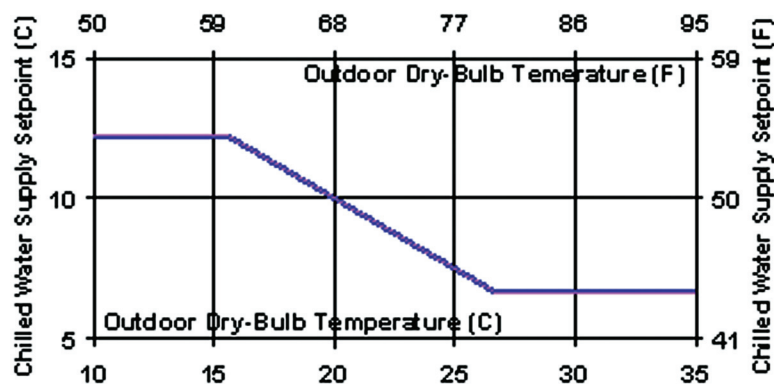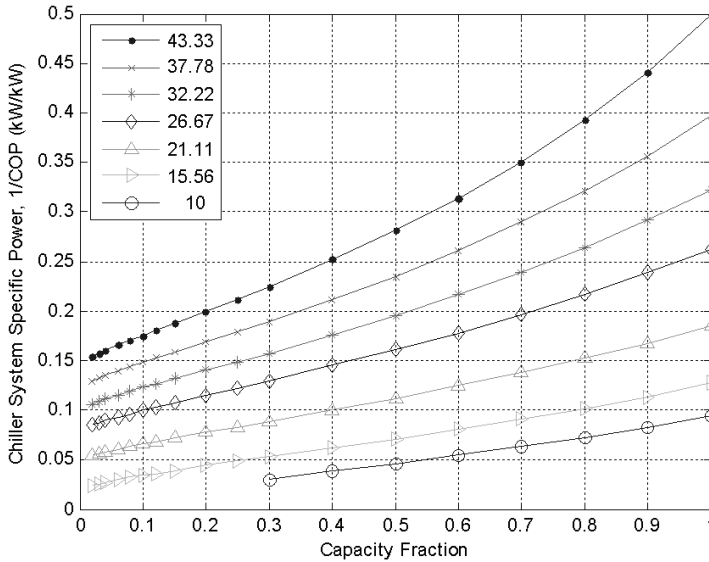**Figure 5. Chiller performance response surface error.**

Figure 6. Chilled-water temperature reset schedule from Appendix G of ASHRAE (1999).

Figure 7. Chiller performance map for the chilled-water reset schedule shown in Figure 6.

Residential Buildings (ASHRAE 1999) was adopted (see Figure 6). Because the chilled-water supply temperature is a function of outdoor dry-bulb temperature, the chiller performance map may still be represented as a black-box function of Q and T_x. This function is shown in Figure 7. Two points should be noted: first, the capacity of the cooling coil is assumed to be adequate (i.e., with the reset schedule of Figure 6, capacity is assumed to be constrained by chilled-water flow rate rather than coil conductance) and second, for the all-air system, supply fan power is not included in the chiller COP numbers represented in Figure 7. The model imbedded in DOE-2.2 that relates fan power to hourly cooling and ventilation loads is used instead to compute annual fan energy. The cross plots in Figure 8 clearly show the effect of the three outdoor temperature ranges defined by the chilled-water reset schedule.

Bicubic functions, fit over each of the three reset schedule ranges, are described in terms of their coefficients and regression statistics in Table 4. The regression coefficient is greater than 0.9998 for all three bicubics. All bicubic terms are retained because removing the least significant term was found to be about double the residual norm. The fact that the bicubics do not intersect exactly at the intended 60°F and 80°F (10.0°C and 15.56°C) boundaries does not affect performance of the 24-hour peak-shifting algorithm.

Cycling Performance of Two-Speed Chillers

The two-speed chiller is assumed to be identical to the variable-speed chiller, except that it can only operate at 0%, 50%, and 100% of rated capacity Q_{Cap}. To satisfy a given hourly load, Q, with a specified outdoor temperature, T_x, the two-speed chiller must cycle on and off to satisfy an hourly load less than 50% of capacity under prevailing conditions. And it must cycle between low- and high-speed operation to satisfy an hourly load greater than 50% of rated capacity. The high-speed duty fraction is given as a function of capacity fraction $y = Q/Q_{Cap}$ by:

$$t_H = 2y - 1 \tag{30}$$

Table 4. Chiller VAV Performance Map Coefficients; $x = T_x$, y = Capacity Fraction

Term	10 < T_x< 15.56°C 50 < T_x < 60°F R^2 = 0.9999		15.56< T_x< 26.67°C 60 < T_x < 80°F R^2 = 0.9999		26.67< T_x< 43.33°C 80 < T_x < 110°F R^2 = 0.9998	
	x in °C	x in °F	x in °C	x in °F	x in °C	x in °F
Constant	–4.24E-02	–2.50E-01	–7.67E-02	–2.64E-01	–1.25E-01	–4.33E-01
x	6.31E-03	1.04E-02	7.78E-03	7.72E-03	1.24E-02	1.27E-02
y	9.24E-02	1.06E-01	1.69E-01	3.96E-01	4.36E-01	8.02E-01
x^2	–2.13E-04	–1.49E-04	–1.20E-04	–6.93E-05	–2.36E-04	–1.10E-04
xy	3.17E-04	–1.00E-03	–7.76E-03	–9.87E-03	–1.59E-02	–1.40E-02
y^2	–6.82E-02	–8.10E-02	–1.03E-01	–1.48E-01	–3.05E-01	–4.32E-01
x^3	5.04E-06	8.65E-07	1.97E-06	3.37E-07	2.23E-06	3.82E-07
x^2y	5.97E-05	1.84E-05	2.82E-04	8.69E-05	2.62E-04	8.07E-05
xy^2	7.17E-04	3.98E-04	2.52E-03	1.40E-03	7.15E-03	3.97E-03
y^3	4.98E-02	4.98E-02	5.18E-02	5.18E-02	1.00E-01	1.00E-01
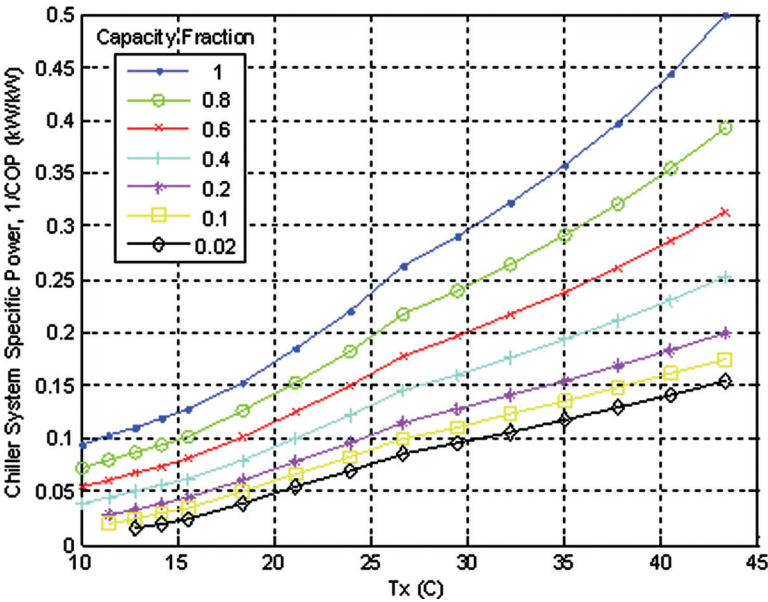
Figure 8. Chiller map cross-plots for the chilled-water reset schedule shown in Figure 6.

and because $t_H < 0$ implies $X < 0.5$, hourly performance is evaluated by the following algorithm:

if $t_H < 0$

$$E_{chiller} = Qf(T_x, 0.5)$$

else

$$E_{chiller} = Q((1 - t_H)f(T_x, 0.5) + t_Hf(T_x, 1.0))$$

where $f(T_x, y)$ is the chiller performance in kW_e/kW_{th} (1/COP) at outdoor temperature T_x and capacity fraction y.

Note that for fan systems, during occupied hours, Q is the coil load, including the sensible and latent load of conditioning the ventilation air with credit for any air-side economizer capacity at prevailing return-air and outdoor-air conditions. For radiant distribution systems with DOAS, as implemented in this study (see DOAS modeling section), Q consists of the building sensible cooling load with two adjustments: 1) net heat rejected by the dehumidifier is added and 2) an air-side economizer credit that is roughly[14] 15% of the all-air system economizer credit under similar conditions is applied. Dehumidifier net heat rejection is defined as the product of supply-return temperature difference and thermal capacitance rate.

Hourly Cycling Performance of Two-Speed Chiller in Unoccupied Hours

The lowest cost response of an all-air system to cooling demand in an unoccupied hour may entail running fans for less than the full hour. To determine the optimal response, the low- and high-speed cooling capacities were evaluated, including economizer capacity Q_{econ} and the corresponding values of chiller power R including fan power in W/W or W/Btu$_h$:

$$Q_L = 0.5Q_{Cap} + Q_{econ}; \quad R_L = P_{fan} + 0.5Q_{Cap}f(T_x, 0.5) \tag{31}$$

$$Q_H = Q_{Cap} + Q_{econ}; \quad R_H = P_{fan} + Q_{Cap}f(T_x, 1.0) \tag{32}$$

where $Q_{econ} = C_{fan}(T_{RA} - T_x)$ is the free-cooling capacity. The high-speed duty fraction is now

$$t_H = \frac{Q - Q_L}{Q_H - Q_L},$$

which reduces to $t_H = 2y - 1$ when $Q_{econ} = 0$. The algorithm must consider the possibility that a cooling load may be satisfied more economically at high-speed than at low because low-speed chiller operation increases the duration of fan operation and associated fan energy is roughly doubled. Conversely, if cooling is most efficiently provided by fan-only operation, the chiller should be operated for the least possible fraction of the hour according to the following algorithm:

if $(R_H/Q_H) < (R_L/Q_L)$

$$E_{system} = (Q/Q_H)R_H$$

else if $t_H < 0$

if $(R_{econ}/Q_{econ}) < (R_L/Q_L)$;

else $E_{system} = (Q/Q_L)R_L$

else

$$E_{system} = Q((1 - t_H)R_L/Q_L + t_HR_H/Q_H)$$

end

---

[14] The credit is not exactly constant because the ratio of latent to total energy recovery varies and because the ratio of DOAS airflow to VAV system airflow varies.

Figure 9. Chiller schematic showing refrigerant-side economizer bypass check valve. If the throttling valve is a float or electrically-actuated valve, the liquid bypass branch is not needed. If condenser elevation is insufficient, a liquid refrigerant pump is needed.

REFRIGERANT-SIDE ECONOMIZER (FREE COOLING)

When it is colder outdoors than in ($T_x < T_z$) the load can be partly or entirely satisfied by using outside air. However, the free-cooling capacity of a DOAS is only about 15% that of an all-air system. One economical and low-maintenance way that hydronic radiant distribution can be used to effect free cooling is to bypass the compressor and pump the liquid refrigerant, or arrange for the liquid to return by gravity from condenser to evaporator, as shown in Figure 9. To evaluate free-cooling transport cost under a given condition, the pressure difference corresponding to the infinite thermal capacitance rate bounds on T_e and T_c must be sufficient to move refrigerant at a rate that will satisfy the cooling load, Q. The performance in economizer mode thus involves the evaporator and condenser external thermal capacitance rates, associated heat exchanger parameters, and associated transport power relations as developed previously for the chiller model. In addition, there is a relation governing the mass flow of refrigerant through or around the compressor, involving the pressure difference corresponding to the evaporating-condensing temperature difference, which must be addressed.

The refrigerant mass flow rate, F, may be modeled by a power law relation:

$$F = c_{Fecon}(\Delta p/\rho)^x \tag{33}$$

where $0.5< x < 1$ depends on the relative importance of laminar and turbulent flow losses.

The relation between evaporating-condensing pressure difference and temperature difference, which depends only on refrigerant properties, is also reasonably well described by a power law. Moreover, the heat rate, given by

$$Q = \min(Fh_{fg}(T_e), Fh_{fg}(T_c)) , \tag{34}$$

is only a weak function of mean temperature. If we define an effective conductance from room to outdoor ambient, $UA_{econ} = Q/(T_z - T_x)$, where Q is given by Equation 34, the total pumping power may be modeled as a compound power law:

$$E_{econ} = c_{Eecon}(UA_{econ})^y (T_z + T_x)^w \tag{35}$$

which corresponds to the following linear model

$$\ln(E_{econ}) = \ln(c) + y \ln(UA_{econ}) + w \ln(T_z + T_x) \tag{36}$$

Asymptotic Behavior. The power law works fine for moderate loads—that is when

$$\frac{T_z - T_x}{Q} = \frac{1}{UA_{econ}} \gg \frac{1}{UA_{max}} = \frac{1}{UA_z} + \frac{1}{UA_e} + \frac{1}{UA_c} . \tag{37}$$

However, transport power begins to rise hyperexponentially as UA_{econ} approaches UA_{max}. A factor that produces the observed asymptotic behavior is required:

$$E_{econ} = c (UA_{econ})^y (T_z + T_x)^w coth ((UA_{max} - UA_{econ})^{.5})^{18} \tag{38}$$

Map-Generating Algorithm. Economizer performance at a given UA_{econ}, T_z, and T_x is determined by a modified version of the chiller model, which solves for the compressor bypass saturation temperature T that minimizes transport power in economizer mode. First, the saturated refrigerant properties P, ρ, and h_{fg} are evaluated at a feasible trial value of T, for example,

$$T = (R_e + R_c)(T_z/R_e + T_x/R_c) , \tag{39}$$

where $R_e = 1/UA_e + 1/UA_z$ and $R_c = 1/UA_c$. The mass flow rate needed to produce the required heat rate and the corresponding pressure drop can then be evaluated:

$$F = Q/h_{fg} \tag{40}$$

$$\Delta p = (F/c_{Fecon})^{1/x} \tag{41}$$

Evaporator and condenser pressures ($P \pm \Delta p /2$) and the corresponding temperatures are evaluated as

$$T_e = T_{sat}(P + \Delta p/2) \tag{42}$$

$$\text{and} \quad T_c = T_{sat}(P - \Delta p/2) \tag{43}$$

and the thermal capacitance rates C_e and C_c and associated transport power requirements are evaluated using the heat exchanger solvers and speed-power-flow rate relations. A bounded search on T finds the minimum transport power solution for a given (T_z and T_x) condition.

Second-Order Effects. The transport properties of air and water are weak functions of temperature.

The refrigerant property, h_{fg}, presents a more complicated picture. To assess this sensitivity, the mapper was run again with a 20°F (11 K) temperature shift affecting only the refrigerant properties. The differences in transport power were less than 2% for all cases in which transport power is less than 0.2 kW/ton (0.05 kW$_e$/kW$_{th}$)—i.e., for all conditions in which refrigerant-side free cooling is more efficient than running the compressor.

A biquadratic function, fit over—and slightly beyond—the range of points where refrigerant-side economizer operation is more efficient than vapor-compression operation, is described in terms of its coefficients and regression statistics in Table 5. In application, the mode of operation in the transition region is determined by evaluating both the vapor-compression and economizer-mode performance maps and applying the lower input power result. The performance curves of Figure 5, presented earlier, were generated by this least-input-power evaluation process.

The refrigerant-side economizer model is used only with the RCS/DOAS-based system; conventional VAV and CV systems use air-side economizer equipment.

DEDICATED OUTDOOR AIR SYSTEM

A simple DOAS enthalpy recovery and dehumidification unit is shown schematically in Figure 10. A large-diameter (low-face velocity) enthalpy wheel is desirable for high effectiveness and low pressure drop (Stiesch 1994). Balanced,[15] constant airflow for the DOAS (implying constant occupancy or constant CO_2 generation) is assumed during occupied hours.[16] For HVAC configurations employing RCS/DOAS equipment, the dehumidification section—implemented here as a variable-speed air-to-air vapor compression machine—must satisfy the entire residual latent load (i.e., the total [building plus ventilation] latent cooling load minus the latent cooling recovered by the enthalpy wheel).

DOASs of both constant- and demand-controlled airflow design are simple and economical. Constant volume operation has two desirable properties: 1) fan and duct systems can be optimized (operating versus first costs) in a straightforward way; and 2) good ventilation efficiency can be achieved using simple, properly sized diffusers to introduce conditioned outdoor air to occupied spaces. Demand-controlled ventilation can be implemented with a variable-speed fan and simple terminal dampers—controlled in an office by a light switch position/occupancy sensor and in a large conference room by a CO_2 sensor. Good ventilation efficiency and modest fan energy savings are thus both achieved by a VAV DOAS.

In practical applications, it is desirable that the supply air temperature be above the zone dew point (to prevent condensation on distribution ducts) and below about 80°F (to avoid

Table 5. Biquadratic Economizer-Mode Performance;
$x = T_x$, y = Capacity Fraction, $r^2 = 0.988$

Term	(x in °F)
Constant	6.485E-01
x	–2.356E-02
y	–6.879E-03
x^2	2.101E-04
xy	1.442E-04
y^2	6.370E-06

---

[15] Nearly balanced airflow—commonly assumed when analyzing the performance of enthalpy recovery ventilation equipment—requires a very tight building to maintain the small (10–20 Pa) positive building pressure considered desirable for air quality and prevention, in summer, of condensation in exterior wall cavities. Factors that make balanced airflow feasible include the following: 1) cost-effective low-infiltration measures, products, and commissioning methods already exist, and 2) economic conditions and well-designed policies that encourage energy efficiency in general will promote improved building envelope performance to roughly the same extent.

[16] In practice, a small but finite rate of dehumidification might be necessary when precooling during unoccupied periods.

discomfort). However, for this scoping study, all condenser heat is rejected back into the supply air stream, thus adding to the sensible cooling load that the main chiller, TES (if present), and RCS distribution elements must remove.[17] In a DOAS dehumidification application, the compressor works against a moderate and fairly constant pressure ratio, and the suction pressure is largely determined by the supply-air dew point (50°F–55°F) needed to satisfy the latent load.

Dehumidifier Model Overview

Dehumidifier performance is evaluated using separate models for the compressor-condenser and a direct expansion (DX) evaporator coil. The dehumidifier load, Q_{DX}, consists of the latent part Q_L and sensible part Q_S, thus:

$$Q_{DX} = Q_L + Q_S = m_{SA} (h_{airIN} - h_{airOUT}) \qquad (44)$$

where

m_{SA}	=	supply air mass flow rate
h_{airIN}	=	ventilation air enthalpy at the evaporator inlet
h_{airOUT}	=	nearly saturated supply air enthalpy setpoint at the evaporator outlet

For a given airflow rate, inlet temperature, and total load, the refrigerant evaporating temperature T_e is strictly increasing with latent load fraction Q_L/Q_{DX}. Under conditions that would result in a partially wetted evaporator coil, models that assume fully wetted or completely dry air-side surfaces return T_e estimates lower than would be returned by a model with separate dry- and wet-surface submodels. However, the wet-surface model estimate of T_e is generally close to
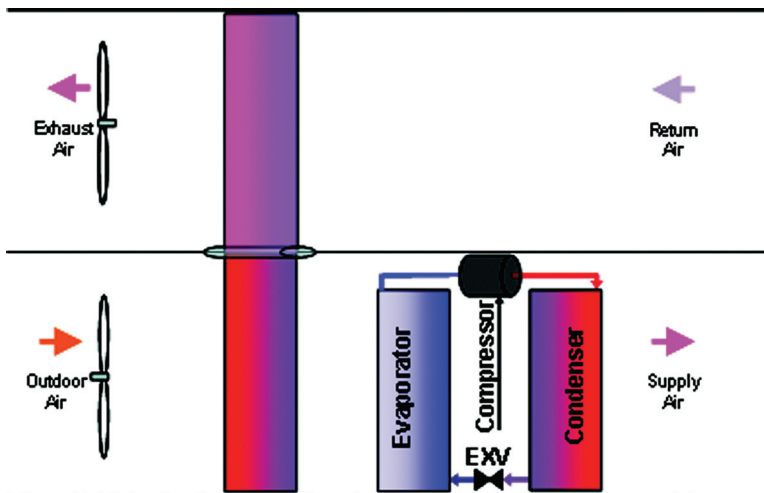
Figure 10. Schematic of the DOAS enthalpy recovery and dehumidification system.

---

[17]This approach has been selected entirely on the basis of simplicity. More efficient schemes are possible including the following: 1) an exhaust-air-cooled auxiliary condenser downstream of the enthalpy wheel with supplementary evaporative cooling fed by the evaporator condensate, 2) vapor compression with a refrigerant mixture that promotes temperature glide, 3) use of a run-around heat exchanger to eliminate most of the sensible load, 4) combinations of the foregoing.

the actual value when any fraction of the coil is wetted (Braun et al. 1989b; Reichler 1999), and in this application, part of the coil is always wet.

Having evaluated T_e and leaving air temperature, the compressor speed and power needed to just satisfy evaporator load with the airflow rate C_{air} required for ventilation in a given hour can be computed. In the arrangement shown in Figure 10, condenser entering air temperature is equal to evaporator leaving air temperature. The compressor and condenser submodels, introduced previously in connection with the main chiller, are used with a DOAS-specific set of equipment parameters to solve for the refrigerant condensing temperature T_c. Note that there is no value in precomputing a performance map. Performance of the DX-dehumidifier is evaluated at most once for each hour in which there is a latent cooling load because the low-lift TES can only address sensible cooling loads. Thus, although dehumidifier operation contributes to building sensible load, it cannot participate in the load-shifting process.

The dehumidifier model has two parts that are evaluated sequentially. Evaporating temperature T_e is first computed based on total coil load Q_{DX} and inlet T_{airIN} and h_{airIN} conditions. The compressor-condenser model then has what it needs, Q_{DX} and T_e, to solve for T_c with compressor speed and refrigerant flow as intermediate variables. The compressor and condenser models have already been derived; the coil model is presented below.

Evaporator Coil

The coil model determines refrigerant evaporating temperature T_e, given load, and entering air temperature T_w. For a zero-superheat dry DX coil, there is only sensible cooling, and the local heat transfer rate is thus given by

$$dQ = U(T_{air} - T_e)dA , \tag{45}$$

where

U	=	air-to-refrigerant thermal conductance per unit area,[18]
dA	=	differential area along the air-side path (from air-side inlet to outlet),
T_e	=	DX coil refrigerant-side evaporating temperature, and
T_{air}	=	temperature of process air, a function of position on the air-side path.

The infinite-NTU DX dry-coil capacity is

$$Q_{max} = C_{air}(T_{airIN} - T_e) , \tag{46}$$

and the effectiveness-NTU model can be used to estimate actual coil capacity as follows:

$$Q = \varepsilon C_{air} (T_{airIN} - T_e) \tag{47}$$

where

$$C_{air} = \text{air-side thermal capacitance rate}$$

$$\varepsilon = 1 - e^{-NTU} \tag{48}$$

$$NTU = UA/C_{air} \tag{49}$$

---

[18] Although any consistent basis area $A = \int dA$ may be used for the integration $UA = \int U dA$, it is customarily taken to be the refrigerant inside tube surface area.

The overall resistance, $1/UA$, is evaluated assuming that the heat transfer rate is controlled by the air- and refrigerant-side resistances, assumed to be uniform over the heat exchanger, thus:

$$\frac{1}{UA} = \frac{1}{(hA)_{air}} + \frac{1}{(hA)_r} \tag{50}$$

where

$1/(hA)_{air}$ = air-side resistance
$1/(hA)_r$ = refrigerant-side resistance

The air-side process with high latent load (fully wetted DX coil) is a combined mass and thermal diffusion process driven by a temperature gradient and a moisture gradient. The gradients are not independent but are linked through the moist air properties (Lewis 1922, 1933; Keevil 1928). Thus, the two gradients may be modeled by a single enthalpy gradient, and the wetted-coil local enthalpy transfer rate is

$$dQ = U_h(h_{air} - h_{airsat}(T_e))dA , \tag{51}$$

where

U_h = effective enthalpy conductance per unit area,
h_s = enthalpy of saturated air evaluated at refrigerant-side evaporating temperature,
h_{air} = enthalpy of process air, a function of position on the air-side path, and
dA = differential area along the air-side path (from air-side inlet to outlet).

The maximum possible wet DX coil capacity is

$$Q_{max} = m_{air}(h_{airIN} - h_{airsat}(T_e)) , \tag{52}$$

and the effectiveness-NTU model estimates actual fully wetted coil capacity as follows:

$$Q = \varepsilon_h m_{air}(h_{airIN} - h_{airsat}(T_e)) \tag{53}$$

where

$$m_{air} = \text{air-side mass flow rate}$$

$$\varepsilon_h = 1 - \exp(-NTU_h) \tag{54}$$

$$NTU_h = \frac{UA_h}{m_{air}} \tag{55}$$

The enthalpy diffusion resistance is defined in terms of equivalent air-side and equivalent refrigerant-side resistances for combined heat and moisture diffusion, thus:

$$\frac{1}{UA_h} \approx \frac{c_{p,air}}{(hA)_{air}} + \frac{c_s}{(hA)_r} \tag{56}$$

where

$$c_s \approx \frac{h_{airsat}(T_{dp,IN}) - h_{airsat}(T_e)}{T_{dp,IN} - T_e} \approx \frac{dh_{airsat}(T_{sw})}{dT_{sw}} \tag{57}$$

and

$T_{dp,IN}$ =   entering air dew point temperature
T_{sw} =   average temperature of wetted surface

Evaluation using Wet- and Dry-Coil Models. The refrigerant evaporating temperature required to satisfy the load is computed using both the dry- and wet-coil models. If the wet-coil model gives a higher T_e, we know that the dry-coil model is invalid, and the coil must be mostly or fully wet. The dry coil model can give a higher T_e only when $Q_L << Q_S + Q_L$ but will nevertheless prove useful. In either case—wet or dry—the mass flow and thermal capacitance rates are first evaluated as follows:

$$m_{air} = \rho_a V_a \tag{58}$$

where ρ_a is standard air density and V_a is the standard volumetric flow rate and

$$C_{air} = c_{p,air} m_{air} \tag{59}$$

Dry-Coil Model. Evaluation of the evaporator saturation temperature required to satisfy a total load, Q, with a small latent load fraction proceeds directly by evaluating Equations 47 through 50 in reverse sequence, thus:

$$\frac{1}{UA} \approx \frac{1}{(hA)_{air}} + \frac{1}{(hA)_r} \tag{50}$$

$$NTU = UA/C_{air} \tag{49}$$

$$\varepsilon = 1 - \exp(-NTU) \tag{48}$$

$$T_e = T_{airIN} - Q/(\varepsilon C_{air}) \tag{47}$$

Wet-Coil Model. There is not a closed form T_e solution for the wet-coil model. However, the DX coil entering air temperature presents an upper bound, and the solution for T_e from the dry coil model provides a lower bound that will generally be close[19] to the wet-coil solution. Equations 53 through 57 may, therefore, be solved by interval bisection as follows:

TUB = T_{airIN}
TLB = $T_{airIN} - Q / (\varepsilon C_{air})$
Iterate 12 times for ~0.01F precision:
         T_e = (TUB + TLB)/2
         $T_{sw} = T_e + Q / (hA)_r$; temperature of wetted surface
         $c_s = dh_{airsat}(T_{sw})/dT$

         $\frac{1}{UA_h} \approx \frac{c_{p,air}}{(hA)_{air}} + \frac{c_s}{(hA)_r}$

         $NTU_h = UA_h/m_{air}$
         $Q_{test} = (1 - \exp(-NTU_h))m_{air} (h_{airIN} - h_{airsat}(T_e))$
         if $Q_{test} > Q$; TLB = T_e
          else; TUB = T_e; endif
  end iteration loop

---

[19] Except when the latent fraction is small. In this case, it is not clear that continuous DX operation over the simulation time step is a good strategy.

Dry Fraction. To validate the approximate solution, we can estimate the fraction of the air-side surface that is dry, x_d, and apply effectiveness-NTU models separately to the dry and wet portions of the DX heat exchanger. Assuming constant T_e on the refrigerant side, the relation between air and surface temperature over the dry portion of the coil (i.e., over $0 < x < x_d$) is

$$T_s(x) = \frac{(hA)_{air}T_{air}(x) + (hA)_r T_e}{(hA)_{air} + (hA)_r} \tag{60}$$

or, equivalently,

$$T_{air}(x) = \frac{((hA)_{air} + (hA)_r)T_s(x) + (hA)_r T_e}{(hA)_{air}}, \tag{61}$$

where $T_s(x_d) = T_{sw}$. The air-side temperature at the dry-wet boundary must also satisfy the dry region approach-temperature relation:

$$\frac{T_{air}(x) - T_e}{T_{airIN} - T_e} = 1 - e^{-xNTU} \tag{62}$$

or, equivalently:

$$\frac{T_{air}(x) - T_{airIN}}{T_{airIN} - T_e} = e^{-xNTU} \tag{63}$$

Thus,

$$x_d = \frac{1}{NTU}\ln\left(\frac{T_{airIN} - T_e}{T_{airIN} - T_{air}(x_d)}\right), \tag{64}$$

in which the previously derived expression in T_{sw} may be substituted for $T_{air}(x_d)$. The effectiveness-NTU dry- and wet-region models thus give total sensible cooling of the airstream as

$$Q_{s,NTU} = (1 - e^{-xNTU})C_{air}(T_{sw} - T_{sw}) + (1 - e^{(x-1)NTUA}) C_{air} (T_{sw} - T_{sw}), \tag{65}$$

where

$$NTUA = (hA)_{air}/C_{air}. \tag{66}$$

Least-Input Power Solution. Interval bisection may be used to search for a solution T_c on the conservatively broad interval[20] $T_{CndEA} < T_c < (T_{CndEA} + Q_{max}/C_{sa})$, where Q_{max} is based on the compressor power at highest permissible saturated condensing temperature. For each trial T_c, the fraction of the condenser needed for desuperheating is determined by interval bisection, as developed previously in the condenser model. The deviation of condensing region air-side capacity[21] from refrigerant-side load then determines which half of the current solution interval is to be eliminated. Upon convergence, the condenser-leaving air temperature is evaluated based on the sum of

---

[20] Note that $T_x < T_c$ and that there can be no ventilation air latent load when $T_x < T_{SADP}$, therefore $T_{SADP} < T_c$; the compressor map limit $T_{cmapmax} = 130°F$ provides an adequate upper bound while being safely below any degenerate solution.

[21] Based on effectiveness-NTU relations and relative portions of the condenser devoted to desuperheating and condensing.

compressor input power and unrecovered ventilation air cooling load $W + Q_{DX}$. The difference between condenser-leaving air temperature and return-air temperature represents the portion of DX-dehumidifier heat rejection rate added to the sensible cooling load of the building.

CONCLUSION

To estimate the energy consumption of a building that uses the baseline HVAC configuration, the full low-lift system configuration, or one of the partial low-lift configurations, a detailed simulation model is needed. Existing detailed simulation models (DOE-2.2, BLAST, and EnergyPlus [Jacobs 2002]) currently lack the capability to simulate any of the low-lift configurations that involve TES and peak-shifting. Moreover, few available compressor and chiller models cover the required range of compressor speed, and neither models nor published data could be found for very low pressure ratio operation. Therefore, component models were developed and used to generate chiller subsystem performance maps that could be incorporated into an hour-by-hour simulation. Performance map models of the chiller-RCS subsystem, chiller-VAV (or chiller-CV) subsystem, and dedicated-outdoor-air subsystem were developed for use with the building cooling loads and fan power loads generated by DOE-2.2. Formulation of component models was guided by the need to make equitable performance comparisons between all-air and RCSs/DOASs, between a building that uses or does not use TES, and between variable-speed and fixed- or multispeed equipment.

A semi-empirical compressor model was developed based on published performance data for an existing reciprocating compressor designed for operation over a 4:1 speed range. Compressors in the model line have similar performance because, for machines rated from 10 to 30 hp (8 to 24 ton or 25 to 75 kW cooling capacity), they differ only in number of cylinders (two to six). The compressor model thus applies broadly to 25 through 75 kW capacity chillers. This and other compressor modeling efforts would benefit greatly from wider availability of measured compressor performance data at low pressure ratios and over a wide range of shaft speed.

Two chiller system models that differ only in the type of distribution were developed. Each chiller system model includes the previously mentioned compressor, an air-cooled condenser and condenser fan, a water-cooled evaporator with chilled-water pump. The two types of distribution are a radiant cooling system and a cooling coil operated according to a standard VAV-system chilled-water supply temperature versus outdoor temperature reset schedule.

The condenser fan and chilled-water pump, as well as the compressor, were modeled with variable-speed controls using both cooling distribution modes of the chiller system solver. The chiller solver is a performance-optimizing model that includes load-side transport power as well as compressor and condenser fan power in its object function. The chiller solver finds the saturated condenser and evaporator refrigerant temperatures that minimize input power given cooling load and the external load-side and outdoor thermal conditions. The mechanism for reducing chiller input power is the adjustment of fan, pump, and compressor speeds to best match saturated condenser and evaporator refrigerant temperatures with chiller load and external conditions. A rigorous solution of the chiller control problem with independently controlled compressor, condenser fan, and chiller water pump speeds was thus achieved by using a quasi-physical compressor model, first-principles models of heat exchanger components, and widely accepted empirical power law models of chilled-water and condenser air transport components.

To fully realize the potential thermodynamic benefits of variable-speed operation, it is crucial to select compressor, fan and pump components, and associated motors that exhibit high efficiencies over a wide speed range. Additional well-understood chiller efficiency measures, assumed for both the variable-speed and baseline chiller designs, include:

- separate cooling of compressor motor so that motor heat is rejected directly to ambient[22]
- low flow loss design of evaporator, condenser, and refrigerant piping
- flooded-evaporator design to achieve very low suction superheat
- use of a liquid receiver to maximize condensing area (very low subcooling)

Full-load performance of the optimal variable-speed chiller is not much different from that of existing chiller systems. However, system COP improves at low capacity fraction relative to existing, duty-fraction-modulated two-speed chiller systems or systems that do not have a wide speed range. The reciprocating compressor was chosen for this analysis because its free discharge and very low back-leakage characteristics are more favorable to variable-speed part-load efficiency than other positive displacement (PD) compressor types. Centrifugal compressors were not considered because PD compressors are more efficient when turndown ratio goes much beyond 2:1.

Three versions of the chiller model were developed to produce the two chiller performance maps. The first performance map is for the chiller RCS system; the map repesents a refrigerant-side economizer as well as compressor operation. The chiller model for economizer operation uses the same components as the chiller for compressor operation except that the compressor is replaced by the flow-pressure characteristic of the compressor bypass branch used during economizer operation. The performance in compressor mode is represented by a bicubic function, and the performance in economizer mode is represented by a biquadratic, both functions of outdoor temperature and capacity fraction. At each performance evaluation, the compressor-mode bicubic is evaluated, and, if outdoor temperature is below room temperature, the economizer biquadratic is also evaluated; the mode of operation (compressor or economizer) is determined by which model returns the better COP.

The chiller-VAV system uses an air-side economizer, so only one chiller model is needed to produce a chiller performance map. However, the map has three regions corresponding to a reset schedule in which chilled-water supply temperature is a piece-wise linear function of outdoor temperature. A separate bicubic was fit to each of the three regions. The compressor, condenser, condenser fan, evaporator, and chilled-water pump used to produce the chiller-VAV subsystem map are identical to those used to produce the chiller-RCS subsystem performance map.

Two-speed chiller-VAV and chiller-RCS subsystem performance curves are derived from the corresponding variable-speed bicubic performance functions. The low- and high-speed specific power curves—functions of outdoor temperature only—are obtained by evaluating the variable-speed performance map at capacity fractions of 0.5 and 1.0. The identical procedure is used for both two-speed-chiller-VAV and two-speed-chiller-RCS subsystems.

A simple model of energy recovery ventilation is provided by DOE-2.2. The remaining latent load is satisfied by a DX dehumidifier modeled as two subsystems: the wetted evaporator coil and a scaled-down version of the variable-speed chiller with heat rejection to the ventilation supply air. The resulting sensible load is added to the building sensible load and can, therefore, be treated as peak-shiftable load. Airflow and fan power are determined by ventilation demand while compressor power is determined by the evaporator inlet conditions and the latent load remaining after enthalpy recovery.

The annual energy simulations use DOE 2.2-generated load sequences to which DOAS reheat has been added for the cases that use DOASs. For systems without TES, the appropriate chiller map is applied directly to the baseline load sequence. For systems with TES, annual energy is evaluated in 365 daily subsimulations and the 24-hour peak-shifting algorithm described at the beginning of this paper applies the appropriate chiller performance map to each 24-hour load

---

[22] Suction-gas cooling may continue to be life-cycle-cost-optimal—even at high electric rates—with compressor motors that use a permanent-magnet (PM) rotor, because PM motor loss is about one-half that of a functionally similar induction motor.

sequence plugged into its objective function. The solution to this subproblem is the 24-hour load sequence that minimizes cooling system input energy for the day in question.

Results from annual simulations reported in the companion paper indicate that chiller, fan, and pump energy savings potential ranges from 60% to 74% for temperate to hot and humid climates and from 30% to 70% in milder climates with high economizer and night free-cooling potential. The savings are calculated as a difference between annual energy use (chiller, fan, and pump) for a building with a conventional HVAC system and annual energy use for the same building with the full low-lift HVAC configuration using the same basic chiller and transport components.

ACKNOWLEDGMENT

NOMENCLATURE

A, dA	=	heat exchanger area, differential area
c	=	C_e/UA_{eff} dimensionless chilled-water flow rate
c	=	constant for refrigerant-side economizer model
C	=	ratio of effective clearance volume to displacement
C_{air}	=	thermal capacitance rate, DOAS supply air
C_c	=	condenser air thermal capacitance rate
C_e	=	chilled-water thermal capacitance rate
C_{flow}	=	constant proportional to effective valve-free area
C_{fan}	=	thermal capacitance rate in all-air system
$[C_{ij}]$	=	$[C_{00}\ C_{01};\ C_{10}\ C_{11}]$ coefficients of polytropic exponent compression process model
C_{min}	=	the lesser of $\rho V(h_o - h_{sd})/(T_{sh} - T_c)$ and xC_c,
COP	=	$f(T_X, T_Z, Q_{Load})$ = chiller coefficient of performance
D	=	effective and actual compressor displacement
dA	=	differential area along heat exchanger air-side path
e_e	=	dimensionless chilled-water supply approach temperature
e_z	=	dimensionless chilled-water return approach temperature
$E_{chiller}$	=	chiller system input power, two-speed operation
E_c	=	condenser fan input power
E_e	=	chilled-water pump input power
E_{econ}	=	chiller input power with compressor off (refrigerant-side economizer mode)
f	=	shaft speed in rotations per second
F	=	Q/h_{fg} refrigerant flow rate, compressor off
$1/(hA)_{air}$	=	air-side resistance
$1/(hA)_r$	=	refrigerant-side resistance
$h(P,v)$	=	enthalpy of refrigerant vapor given pressure and specific volume
h_{airIN}	=	ventilation air enthalpy at evaporator inlet and outlet
h_{airOUT}	=	ventilation air enthalpy at evaporator inlet and outlet
h_c	=	saturated vapor enthalpy at P_o
$h_{DXINLET}$	=	ventilation air enthalpy at evaporator inlet
h_e	=	saturated vapor enthalpy at P_i

h_{fg}	=	enthalpy of vaporization evaluated at mean of evaporating and condensing temperatures
h_i	=	inlet enthalpy (at P_i and T_i)
h_{liq}	=	saturated liquid enthalpy at P_o
h_o	=	outlet enthalpy (at P_o and T_o)
$h_{airsat}(T)$	=	enthalpy of saturated air evaluated at refrigerant-side evaporating temperature
h_{SA}	=	nearly saturated supply air enthalpy setpoint at the evaporator outlet
J	=	variable-speed chiller system input power
k_{FSx}	=	condenser fan $x = e$ and condenser fan $x = c$ thermal capacitance rate at rated speed
k_{PSx}	=	chilled-water pump $x = e$ and condenser fan $x = c$ power at rated speed
m_{air}	=	DOAS DX dehumidifier coil air-side mass flow rate
m_{SA}	=	supply air mass flow rate
n	=	polytropic exponent based on empirical compression process model
n_{IG}	=	c_p/c_v volume exponent for ideal gas in isentropic (adiabatic, reversible) compression
n_T	=	1 = volume exponent for ideal gas with heat removed during compression (isothermal)
n_s	=	volume exponent for isentropic compression of real gas
NTU	=	UA/C_{air} number of transfer units based on air-side thermal capacitance rate
NTU_h	=	$(UA)_h/m_{air}$ number of transfer units for combined heat and moisture diffusion
P_d	=	discharge pressure assumed equal to outlet pressure
P_i	=	compressor inlet pressure
P_o	=	compressor outlet pressure
P_s	=	suction pressure in cylinder during suction stroke (lower than inlet pressure)
Q	=	evaporator heat rate—positive for cooling
Q_{Cap}	=	chiller cooling capacity at full speed operation—a function of outdoor temperature

Q_{DX}	=	$Q_L + Q_S = m_{SA}(h_{DXINLET} - h_{SA})$DOAS DX evaporator cooling load
Q_H	=	chiller cooling capacity in high-speed operation
Q_L	=	chiller cooling capacity in low-speed operation
Q_{Load}	=	building cooling load with no peak-shifting
Q_{sh}	=	desuperheating portion of condenser load
$Q_{s,NTU}$	=	sensible cooling of DOAS supply air by DX coil
R	=	ratio of minimum to maximum thermal capacitance rate
R_e	=	$1/UA_e + 1/UA_z$, $R_c = 1/UA_c$ refrigerant-side economizer infinite-capacitance-rate resistances
R_H	=	chiller-specific input power at high-speed operation
R_L	=	chiller-specific input power in low-speed operation
SST	=	T_e = saturated suction temperature
SDT	=	T_c = saturated discharge temperature
SSH	=	$T_i - T_e$ = suction superheat
T_H	=	$2X - 1 = (Q - Q_L)/(Q_H - Q_L)$ chiller high-speed duty fraction
T	=	$(R_e + R_c)(T_z/R_e + T_x/R_c)$ initial mean refrigerant temperature estimate
T_{air}	=	DOAS DX dehumidifier local air-side temperature
T_{airIN}	=	ventilation air temperature at evaporator inlet
T_c	=	saturated discharge or condensing temperature; temperature at the desuperheater exit[23]
T_{cwr}	=	chilled-water return temperature
T_{cws}	=	chilled-water supply temperature
$T_{dp,INLET}$	=	entering air dew point temperature
T_e	=	evaporating temperature[17]
T_{LAT}	=	condensing section leaving air temperature
T_{sh}	=	T_o = compressor discharge temperature (superheated)
$T_s(x)$	=	local temperature of surface of DOAS DX-dehumidifier coil

[23] T_c and T_e are used in the DOAS DX-dehumidifier model as well as the chiller model

$T_{sw} \sim T_s(x_d)$	=	average temperature of wetted surface of DOAS DX-dehumidifier coil	V	=	refrigerant volumetric flow rate
T_x	=	outdoor dry-bulb; condenser air-side inlet temperature	$v(P,s)$	=	specific volume of refrigerant vapor given pressure and entropy
T_z	=	room (zone) temperature	W	=	compressor shaft input power
u_e	=	UA_e/UA_{eff} = evaporator parameter	w	=	temperature exponent of chiller input power model for refrigerant-side economizer mode
u_z	=	UA_z/UA_{eff} = RCS parameter	X	=	Q/Q_{Cap} = capacity fraction for evaluating two-speed chiller hourly input power
U	=	thermal conductance per unit area			
UA_h, U_h	=	enthalpy conductance and conductance per unit area for heat and moisture diffusion	x	=	fraction of condenser devoted to desuperheating
UA_c	=	condenser infinite-flow conductance	x	=	pressure ratio exponent of polytropic model; shaft speed exponent of mass flow model
UA_e	=	evaporator infinite-flow conductance			
UA_z	=	radiant panel array infinite-flow conductance	x_d	=	dry fraction of DOAS DX-dehumidifier coil; $x < x_d$ refers to position of local air-side state
UA_{eff}	=	$Q(T_z - T_e)$ = effective conductance of RCS-evaporator-chilled-water loop system	y	=	conductance exponent of chiller input power model for refrigerant-side economizer mode

Greek Symbols

ρV	=	refrigerant mass flow rate	η_{CV}	=	compressor volumetric efficiency
ρ_i	=	compressor inlet density			
ε	=	heat-exchanger effectiveness	η_{motor}	=	compressor motor and drive efficiency
ε_h	=	DOAS DX heat-exchanger effectiveness for combined heat and moisture diffusion	η_s	=	$W/W_{isentropic}$ = isentropic compression efficiency

REFERENCES

Armstrong, P., W. Jiang, D. Winiarski, S. Katipamula, and L.K. Norford. 2009. Efficient low-lift cooling with radiant distribution, thermal storage and variable-speed chiller controls—Part II: Annual energy use and savings estimates. *HVAC&R Resarch* 15(2):402–33.

ASHRAE. 1999. *ANSI/ASHRAE/IESNA Standard 90.1-1999, Energy Standard for Buildings Except Low-Rise Residential Buildings*. Atlanta: American Society of Heating, Refrigerating and Air-Conditioning Engineers, Inc.

ASHRAE. 2004. *ANSI/ASHRAE/IESNA Standard 90.1-2004, Energy Standard for Buildings Except Low-Rise Residential Buildings*. Atlanta: American Society of Heating, Refrigerating and Air-Conditioning Engineers, Inc.

Baldwin, S.F. 1988. The materials revolution and energy-efficient electric motor drive systems. *Ann. Rev. Energy* 13(67):94.

Boeswirth, L., and V. Milovanova. 1998. Simple but efficient methods for estimation of valve loss, capacity loss due to suction valve throttling and heat transfer in cylinder. Int'l Compressor Engrg. Conf., Purdue University, West Lafayette, IN.

Braun, J.E., J.W. Mitchell, and S.A. Klein. 1987a. Models for variable-speed centrifugal chillers. *ASHRAE Transactions* 93(1): 1794-1813.

Braun, J.E., J.W. Mitchell, and S.A. Klein. 1987b. Performance and control characteristics of a large cooling system. *ASHRAE Transactions* 93(1):1830–52.

Braun, J.E., S.A. Klein, W.A. Beckman, and J.W. Mitchell. 1989a. Methodologies for optimal control of chilled water systems without storage. *ASHRAE Transactions* 95(1):652–62.

Braun, J.E., S.A Klein, and J.W Mitchell. 1989b. Effectiveness models for cooling towers and cooling coils. *ASHRAE Transactions* 95(2):164–74.

Conroy, C.L., and S.A. Mumma. 2001. Ceiling radiant cooling panels as a viable distributed parallel sensible cooling technology integrated with dedicated outdoor-air systems. *ASHRAE Transactions* 107(1).

Gosling, C.T. 1980. *Applied Air Conditioning and Refrigeration*. London: Applied Science Publishers.

Granryd, E. 1998. Power for fans and pumps in heat exchangers of refrigerating plants. Int'l Refrigeration Conf., Purdue University, West Lafayette, IN.

Henze, G., R. Dodier, and M. Krarti. 1997. Development of a predictive optimal controller for thermal energy storage systems. *HVAC&R Research* 3(3):233–64.

Henze, G., and M. Krarti. 1999. The impact of forecasting uncertainty on performance of a predictive optimal controller for thermal energy storage systems. *ASHRAE Transactions* 105(1): 553.

Hiller, Carl C. 1976. *Improving Heat Pump Performance via Compressor Capacity Control,* PhD Thesis, MIT Dept. of Mechanical Engineering, Cambridge, MA.

Jacobs, P., and H. Henderson. 2002. State-of-the-art review—Whole building, building envelope, and HVAC component and system simulation and design tools. ARTI-21CR-305-30010-30020, Final Report, Air Conditioning and Refrigeration Technology Institute, Arlington, VA.

Jahnig, D.I., D.T. Reindl, and S.A. Klein. 2000. A semi-empirical method for representing domestic refrigerator/freezer compressor calorimeter test data. *ASHRAE Transactions* 101(2). See also http://minds.wisconsin.edu/handle/1793/7683.

Jin, H., and J.D. Spitler. 2002. A parameter estimation based model of water-to-water heat pumps for use in energy calculation programs, *ASHRAE Transactions* 108(1).

Keevil, C.S., and W.K. Lewis. 1928. Dehumidification of Air. *Ind. Eng. Chem* 20(10):1058–60.

King, D.J., and R.A. Potter. 1998. Description of a steady-state cooling plant model developed for use in evaluating optimal control of ice thermal energy storage systems. *ASHRAE Transactions* 104(1):42–53.

Lewis, W.K. 1922. The evaporation of a liquid into a gas. *Trans. ASME* 44:325.

Lewis, W.K. 1933. The evaporation of a liquid into a gas—a correction. *Trans. ASME* 55:1567.

Moran, M.J., and H.N. Shapiro. 1995. *Fundamentals of Engineering Thermodynamics*. Hoboken, NJ: Wiley.

NIST. 2007. Standard Reference Database 23—NIST Reference Fluid Thermodynamic and Transport Properties Database (REFPROP 7.0), National Institute of Standards and Technology.: www.nist.gov/srd/nist23.htm.

Popovic, P., and H.N. Shapiro. 1995. A semi-empirical method for modeling a reciprocating compressor in refrigeration system. *ASHRAE Transactions* 101(2):367–82.

Reichler, Mark. 1999. Modeling of rooftop packaged A/C equipment. Masters thesis, Department of Mechanical Engineering, University of Wisconsin–Madison, Madison, WI. http://minds.wisconsin.edu/bitstream/1793/7672/1/Thesis.pdf.

Singh, R., J.J. Nieter, and G. Prater, Jr. 1986. An investigation of the compressor slugging phenomenon. *ASHRAE Transactions* 92(4):250–58.

Stiesch, G. 1994. *Performance of rotary enthalpy exchangers*. Masters thesis, Department of Mechanical Engineering, University of Wisconsin–Madison, Madison, WI. http://sel.me.wisc.edu/theses/Stiesch.zip.

Stoecker, W.F. 1982. *Refrigeration and Air-Conditioning*. New York: McGraw-Hill.

Threlkeld, J.L. 1970. *Thermal Environmental Engineering*, 2d ed. Englewood Cliffs, NJ: Prentice-Hall.

Villadsen, V., and F.V. Boldvig. 1981. Reciprocating compressor design for high efficiency. *ASHRAE Transactions* 87(1):819–25.

Zhu, L.G. 2006. A new integrated design platform for energy-efficient motor control. China Power Supply Society CIB Expo, November 6–7, Shanghai, China.